ARTICLE

SCIENCE CHINA Earth Sciences
earth.scichina.com link.springer.com
https://doi.org/10.1007/s11430-026-2006-9

Climate-Driven trends and spatial variability in oceanic dimethyl sulfide concentration and flux

Lyu YAN & Wei-Lei WANG*

State Key Laboratory of Marine Environmental Science, College of Ocean and Earth Sciences, Xiamen University, Xiamen 361102, China

* Corresponding author (email: weilei.wang@xmu.edu.cn)

Received 7 February 2026; Revised 5 June 2026; Accepted 17 June 2026; Published online 9 September 2026

Abstract Marine dimethyl sulfide (DMS), a climatically active gas generated through degradation of dimethylsulfoniopropionate (DMSP), plays a key role in the Earth's climate system by modifying its radiation budget. However, simulations from Earth System Models (ESMs) provide divergent sea-to-air flux trends, and therefore future variations under climate change are still uncertain. Here, we developed an artificial neural network (ANN) model trained using DMS observations and eight observational environmental parameters, along with model parameters extracted from the simulations of CESM2-WACCM to predict variations of DMS concentrations and sea-to-air flux for both historical (1850–2014) and SSP5-8.5 scenarios (2015–2100). Our simulation shows that the global mean DMS concentration generally declines by the end of this century. Specifically, from 2015 to 2050, it is projected to decrease at a rate of −0.62±0.03% per decade, and the rate reduces to −0.53±0.02% per decade from 2050 to 2100. However, the global mean sea-to-air DMS flux is projected to increase at a rate of 0.61±0.06% per decade from 2015 to 2050, while from 2050 to 2100, the flux increases at an accelerating rate of 1.06±0.04% per decade, mainly driven by the joint effect of increasing sea surface temperature (SST) and wind speed, along with declining sea ice coverage. We further explore the attribution of DMS changes by running a series of sensitivity tests. We find that elevated SST and photosynthetically active radiation (PAR), along with nutrient depletion, lead to the decline in DMS concentrations. Furthermore, our geospatial analysis indicates that mixed layer depth (MLD) emerges as the predominant driver in the Southern Ocean, nutrient-dependent effects strongly correlate with DMS in the open seas (trades and westerlies), and sea surface salinity (SSS) exerts a dominant control on DMS within coastal regions. Our findings suggest that site-specific modeling schemes are needed to accurately model DMS dynamics.

Keywords Marine dimethyl sulfide, Sea-to-air flux, Artificial neural network, Temporal variation

1. Introduction

Oceanic dimethyl sulfide (DMS) is primarily synthesized in seawater through the enzymatic cleavage of the biogenic compound dimethylsulfoniopropionate (DMSP) and released through microalgae exudation and mortality (Stefels, 2000; Simó and Dachs, 2002; Galí et al., 2015). DMS in the surface ocean is supersaturated compared to its atmospheric counterpart, and the sea-to-air flux is responsible for more than half of the total flux of gaseous sulfur to the atmosphere (Quinn and Bates, 2011; Lana et al., 2012). Once in the atmosphere, DMS is oxidized to sulfuric and methane-sulfonic acids, which contribute to the formation of cloud condensation nuclei (CCN) and facilitate cloud formation, and thereby have the ability to reduce solar radiation and affect the Earth's energy budget (Charlson et al., 1987). The CLAW hypothesis postulates a climate-negative feedback loop among phytoplankton, DMS emissions, CCN, and Earth's energy budget. In the proposed feedback loop, CCN and cloud albedo are regulated up or down by oceanic phytoplankton through the medium of DMS emissions (Charlson et al., 1987).

However, the conventional view of DMS induced negative climate feedback is increasingly challenged by emerging evidence. Both model simulations and mesocosm studies suggest that DMS may instead exert a positive climate feedback effect under global warming scenarios (Six et al., 2013; Webb et al., 2016; Wang et al., 2018; Zhao et al., 2024). CO_2 forcing simulations have been conducted to predict DMS distribution and its global-scale emissions, with varying forcing conditions revealing substantial spatial heterogeneity (Bopp et al., 2003; Gabric et al., 2013). As a result of the combined effects of ocean acidification and climate change, the projection of global DMS emissions decreases by about 18(±3)% in 2100 compared to the pre-industrial levels in Earth system model (ESM) climate simulations (Six et al., 2013). Similarly, global mean DMS concentrations are predicted to decrease by 15.1% by the end of this century compared to the historical results (1960–2014), which is believed to be primarily driven by rising CO_2 levels (Zhao et al., 2024). In addition, the declining trend in DMS concentrations and sea-to-air flux under the RCP 8.5 scenario is also projected using a fully coupled Earth system model (CESM)(Wang et al., 2018).

An ensemble of four ESMs (CNRM-ESM2-1, MIROC-ES2L, NorESM2-LM, and UKESM1-0-LL) from the CMIP6 historical and Shared Socioeconomic Pathway 5–8.5 W/m^2 radiative forcing by 2100 (SSP5-8.5) experiments provided divergent trends in DMS concentrations and sea-to-air flux starting from the year of

Citation: Yan L, Wang W L. 2026. Climate-Driven trends and spatial variability in oceanic dimethyl sulfide concentration and flux. Science China Earth Sciences, https://doi.org/10.1007/s11430-026-2006-9

2015, which means that there is significant uncertainty regarding the changes of projected DMS trends based on ESMs in the future (O'Neill et al., 2016; Bock et al., 2021). A recent study by Joge et al. (2025) found that the global mean concentration of surface DMS exhibits a decreasing trend with warming. However, in contrast to the decreasing trend of DMS concentration, the combined effects of increasing wind speed and sea surface temperature, along with decreasing ice coverage lead to an increasing trend of sea-to-air DMS flux. Consensus has not been reached regarding future trends in DMS concentrations and sea-to-air flux. Key factors controlling DMS variations have yet to be determined. Consequently, the response of DMS concentration/flux under a warming climate remains uncertain.

To predict global DMS concentrations and temporal variations, we train an artificial neural network (ANN) model using DMS measurements (Appendix Fig. S1) along with eight observational environmental variables, including Chl a, mixed layer depth (MLD), dissolved inorganic nitrate (DIN), photosynthetically active radiation (PAR), dissolved inorganic phosphorus (DIP), silicate (SiO), sea surface salinity (SSS), and sea surface temperature (SST). Subsequently, we feed the model (Fig. S2) with the monthly outputs from Community Earth System Model version 2 coupled with the Whole Atmosphere Community Climate Model (CESM2-WACCM) historical and SSP5-8.5 experiments. Furthermore, we investigate the mechanisms driving the variations of DMS concentrations under global warming scenarios. We also conduct a series of sensitivity tests to explore the attribution of DMS changes in a warming climate state, and identify the key factors (SST, PAR, and nutrients) in different regions. In the end, we make prospects and suggestions for future study.

2. Data and methods

2.1 Observations

Observational DMS concentration data were obtained from the DMS-Rev3 datasets (Hulswar et al., 2022). Before training the ANN model, we conducted multi-step preprocessing on the data. To avoid data aggregation bias caused by clustering multiple data points within a narrow temporal and spatial range (Obtained within the same day and at the same latitude and longitude), daily averaging was performed on these data points to obtain a daily representative value. A total of 837,265 valid data points were ultimately retained in this stage (see Fig. S1A). The Global Surface Seawater DMS Database also provides additional information, including *in-situ* longitude, latitude, and sampling time. We match DMS concentration with the environmental parameter values accordingly to monthly climatology auxiliary data (Appendix Table S1). For example, DMS measurements were spatially and temporally matched to Terra-MODIS monthly averaged Level 3-binned Chl a and PAR data (4 km resolution; last access: 4 Aug 2025) from February 2000 to January 2025. Climatological MLD data were downloaded from the Monthly Isopycnal/Mixed-Layer Ocean Climatology (MIMOC; Schmidtko et al., 2013). Nutrients (nitrate, phosphate, silicate) data were obtained from the World Ocean Atlas 2023 (WOA2023). All ancillary data were aligned with DMS measurements based on sampling location and time of the month. Rigorous quality control was applied following Galí et al. (2015). For instance, measurements with DMS concentrations below 0.1 nmol/L or exceeding 100 nmol/L are excluded. Coastal data (salinity<30), as well as measurements with anomalously low nutrient concentrations (phosphate<0.01 μmol/L; nitrate<0.01 μmol/L; silicate<0.1 μmol/L) and low Chl a values (Chl a<0.01 mg m^{-3}) were excluded. After quality control, a total of 770,554 observational data points were used for training the ANN model.

A potential limitation of this study is the temporal mismatch between DMS observations and environmental predictors. Although DMS measurements are made at specific sampling times, several environmental parameters used here are monthly climatological fields. This mismatch may introduce uncertainty and reduce the model's ability to capture short-term variability in DMS concentrations, particularly in highly dynamic regions where physical and biological conditions can change rapidly over synoptic to submonthly timescales. The daily averaged DMS concentration characterizes the mean state rather than individual instantaneous observations. This approach minimizes the influence of extreme samples to some extent and effectively filters out daily-scale random perturbations. In addition, the daily representative values of DMS concentration in most grid cells of 1°×1° contain more than one measurement (see Fig. S1B), enhancing the statistical robustness and spatial representativeness of the dataset. Preserving daily observations within each grid, rather than further averaging them to monthly timescales, can maximize the utilization of scarce *in situ* DMS measurements. Meanwhile, the model output is also designed at monthly resolution, making it more consistent with the temporal resolution of the climatological predictors. Nevertheless, this averaging cannot fully resolve variability associated with episodic events, mesoscale processes, or rapid bloom dynamics. Future studies using time-matched satellite products, reanalysis fields, or concurrent *in situ* environmental measurements may further improve the representation of short-term DMS variability and reduce potential biases in dynamic ocean regions.

2.2 Earth system models

For the input data to our ANN model, we used the surface and monthly environmental outputs from the CESM2-WACCM (Danabasoglu et al., 2020). This model was selected because it provides all the environmental parameters required by our ANN model and also contains all variables (wind speed, ice coverage, and SST) needed to calculate DMS flux under both historical and future (SSP5-8.5) scenarios. This is also because of its satisfactory performance in simulating key factors when compared to observational data, as illustrated in Fig. S3. Among the eight environmental parameters, six parameters in CESM2-WACCM achieve the highest R^2 values across all the seven ESMs. For the remaining two parameters (DIP and SST), DIP yields a R^2 value of 0.74, slightly below the maximum R^2 value of 0.78 in NorESM2-LM, while SST achieves 0.97, closely approaching the toppest R^2 value of 0.98. In addition, this particular model ensemble contains multiple ensemble members in both historical and future (SSP5-8.5) scenarios (Table S2). Thus, we can achieve more robust prediction results through ensemble averaging than by relying on any single model.

We then compare our predicted DMS concentrations and DMS flux with the outputs from four ESMs in CMIP6 (CNRM-ESM2-1, MIROC-ES2L, NorESM2-LM, UKESM1-0-LL), further details on the four ESMs are provided in Table S2.

2.3 Artificial neural network model

The ANN model is a branch of artificial intelligence (AI), which is built with a fully connected network of nodes and neurons (see Fig. S2). Each neuron has an activation function and is connected to other neurons by iteratively determined weights (Gardner and Dorling, 1998). This algorithm offers significant advantages as it makes no prior assumptions on the data distribution and can fit data in the gap area using non-linear equations (Gardner and Dorling, 1998; Breiman, 2001). Our ANN model is trained using the Keras deep-learning toolbox in Python 3.8, with eight environmental variables (Chl a, MLD, DIN, DIP, PAR, SiO, SST, and SSS) as predictors and DMS as a predictand. All data are log transformed and normalized to the range of [−1,1].

The dataset is then divided into two groups: Training dataset (616,443 data points) and validation dataset (154,111 points). In the training process, we adjust the hyper-parameters, such as dropout ratio, number of hidden layers, and number of nodes on each layer to prevent overfitting while achieving the best goodness of fit to observations. Eventually, the final ANN model adopted consists of one input layer, two dense hidden layers, and one output layer. The input layer comprises nodes corresponding to the predictors. Each hidden layer contains 128 nodes, and the output layer has a single node for DMS concentration simulations. To mitigate overfitting, two dropout layers with a dropout ratio of 0.25 are incorporated into each hidden layer. Additionally, a L2 kernel regularizer with a regulation parameter value of 0.001 is applied to each hidden layer, this model configuration is referenced from Wang et al. (2020).

2.4 Sea-to-air flux of DMS

DMS flux is calculated using an empirical formula, which takes into account sea surface wind (SSW), sea ice coverage, and the viscosity coefficient related to gas transfer velocities in the atmosphere and surface ocean.

Air-sea gas transfer is estimated using the following bulk formula:

$$F = K_w(C_w - C_a/\mathrm{H}) \quad (1)$$

where F is sea-to-air gas exchange flux, C_w and C_a are bulk water and gas concentrations, and K_w (cm h^{-1}) is the overall gas transfer velocity, expressed in waterside units (Liss and Slater, 1974). K_w reflects the combined resistance to gas transfer on both sides of the interface, as follows:

$$\frac{1}{K_w} = \frac{1}{k_w} + \frac{\mathrm{H}}{k_a} \quad (2)$$

where the dimensionless H is the Henry law constant (gas or liquid), and k_a and k_w are gas transfer velocities in air and seawater, respectively. Our study uses the parameterization for K_w from Joge et al. (2025) (hereafter Joge2025), which is derived through regression linking wind speed and SST. The SST, SSW, and sea-ice fraction (f_{ice}) data are all from the CESM2-WACCM monthly simulation datasets. For DMS concentration in the surface ocean is strongly supersaturated with respect to that in the overlying atmosphere ($C_w >> C_a$), thus the DMS flux bulk formula is simplified finally as:

$$F = K_w \times C_w \times \left(1 - f_{ice}\right) \times 0.24 \quad (3)$$

2.5 Sensitivity tests and correlation analyses

To identify the environmental parameter(s) driving the temporal variations of DMS concentrations as simulated by the ANN model, we conducted a suite of eight sensitivity experiments adhering to a strict control variable framework. In each experimental configuration, seven of the eight prognostic environmental parameters required as ANN input fields were held fixed at their initial historical baseline values (the value for the baseline year of 1850), thereby suppressing any variability not directly associated with the parameter being examined. The sole remaining variable was permitted to vary according to the historical and SSP5-8.5 scenario simulations. This design ensures that any simulated deviation in DMS concentration from the fixed parameter baseline can be attributed exclusively to the temporal trajectory of the single perturbed field. These eight experiments are denoted as VChl, VMLD, VDIN, VPAR, VDIP, VSiO, VSSS, and VSST, representing the single varying parameter of Chl a, MLD, DIN, PAR, DIP, SiO, SSS, and SST, respectively. The resulting experiments thus establish a conceptual understanding, identifying which environmental parameters dominate the projected variation in DMS concentrations under the warming scenario.

We use the Pearson correlation coefficients to represent the spatiotemporal dynamics of the relationship between DMS concentrations and key environmental variables. Comparative Pearson correlation analyses were conducted for both historical (1850–2014) and future (2015–2100) periods. Over the full temporal range of each period, Pearson correlation coefficients (r) were derived to assess the strength and sign of covariation, with $r>0$ representing positive co-variability and $r<0$ an inverse relationship. Statistical significance was determined using a two-tailed Student's t-test, with significance ascribed at $p<0.05$.

3. Results and discussion

3.1 Long-term trends of DMS under global warming scenario

The ANN model captures the major variance in the observational data with a goodness-of-fit R^2 value of 0.81 for both the training and testing datasets (Fig. S4). We subsequently conduct temporal simulations by feeding the ANN model with input parameters extracted from CESM2-WACCM. Our simulation results reveal that higher DMS concentrations are predominantly distributed in the Southern Ocean and the equatorial Pacific region (Fig. S5). Compared with historical distributions, the model reveals distinct trends in DMS concentrations across the global ocean, with notable patterns emerging in several key areas (Fig. 1A). For instance, DMS concentrations exhibit an increasing trend in the Arctic Ocean, the eastern equatorial Pacific, the Indian Ocean, and the southeastern Atlantic, with the highest concentration increase occurring in the adjacent to the east coast of Africa between 0° and 40°S.

Nevertheless, a decreasing trend in DMS concentrations is evident in the low-to-middle latitude regions of the Pacific and Atlantic (especially in the subpolar North Atlantic), with the highest concentration decrease occurring in the Southern Ocean (south of 40°S). This is particularly important because the Southern Ocean is far from anthropogenic aerosol sources, and oceanic DMS is the major source of atmospheric sulfur. There-

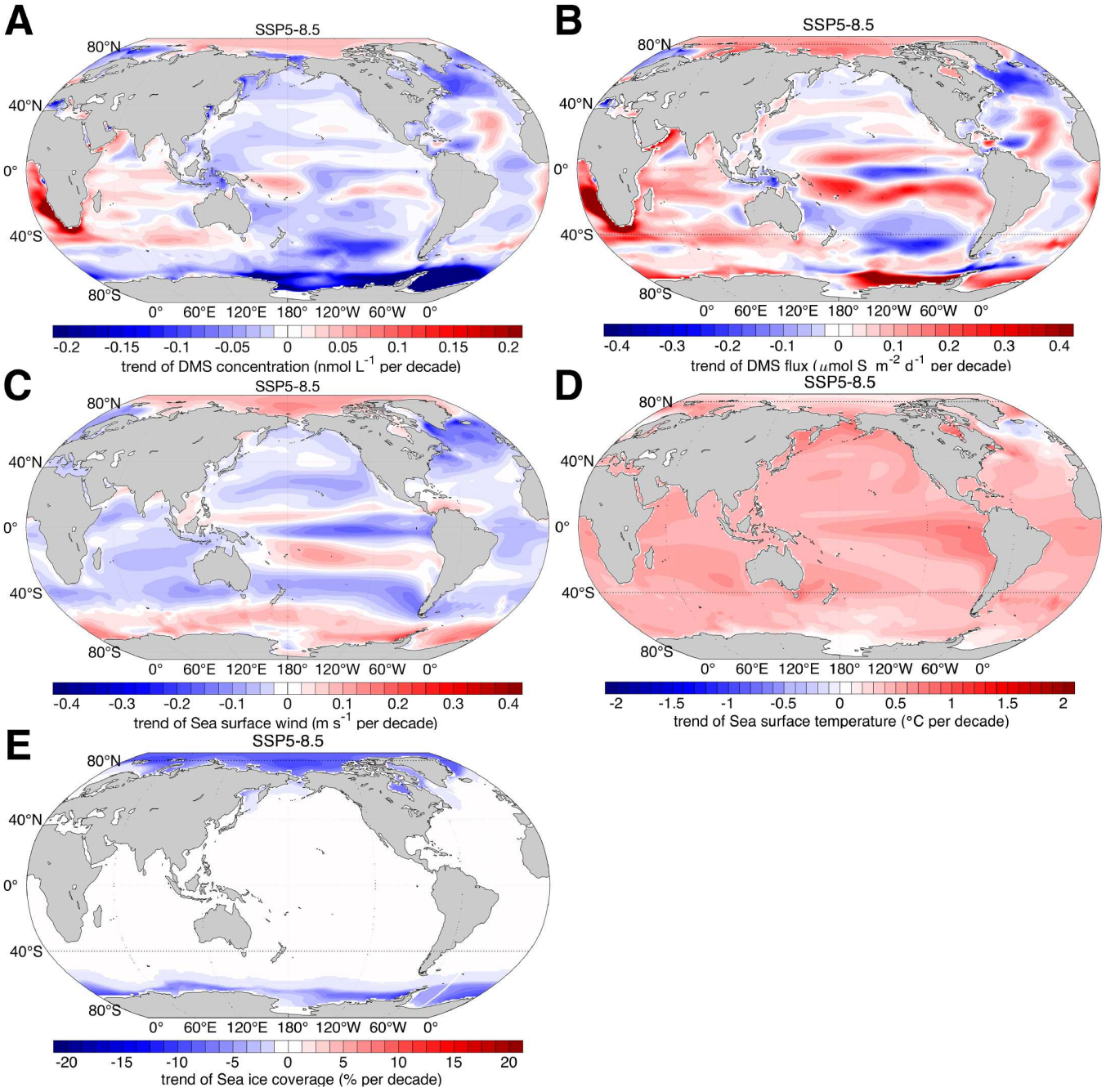

Fig. 1 Trends of DMS concentration and flux with assimilatory parameters from 2015 to 2100 under SSP5-8.5 simulation. (A) trends of DMS concentration; (B) DMS flux; (C) sea surface wind speed; (D) sea surface temperature; and (E) sea ice coverage.

fore, it strongly influences the radiative budget in the Southern Hemisphere (Hamilton et al., 2014).

Using a similar network model, Joge et al. (2025) found that DMS concentrations increase in the subtropical gyres, whereas we observe an opposite trend in the same regions. The discrepancy is primarily attributed to two factors: (1) Data sources: We trained our model using predominantly observational parameters, while Joge et al. (2025) used model outputs. It is well established that ESMs exhibit systematic biases in key DMS relevant variables, including MLD, PAR, and phytoplankton functional type distributions. Because the relationship between DMS concentrations and their environmental drivers is nonlinear and sensitive to these biases, we contend that our ANN model trained on observational data is more likely to capture the realized sensitivity of DMS than those derived from simulated internal model states. (2) Model Ensembles: We employed output solely from CESM2-WACCM as input to our network model, whereas Joge et al. (2025) used an ensemble of eight models. While an ensemble approach is generally robust for bracketing uncertainty at the global scale, it is not necessarily optimal for capturing biogeochemical trends driven by regional parameterizations of marine ecology and air-sea exchange. The variance

introduced by models with lower project skill may attenuate the signal from the more accurate ensemble members. In the specific case of subtropical gyres, where oligotrophic and strong stratification render DMS production is acutely sensitive to changes in nutrient stoichiometry. As illustrated in Fig. S3, CESM2-WACCM demonstrated the best reproduction of observational data among all models considered. The single model may yield a more accurate perspective than the multi-model ensemble. Therefore, the differences in data sources and model ensembles likely account for the divergent results observed in DMS concentration trends.

The sea-to-air flux of DMS generally follows a similar trend to DMS concentrations. The correlation sign is consistent in most of the open oceans, except for regional discrepancies in coastal biomes. These discrepancies are probably caused by the inverse change of wind speed with DMS concentrations.

To elaborate more on the trend of DMS with global warming, we calculate the global area-weighted annual mean DMS concentrations and DMS flux from 1850 to 2100. The temporal trend from our ANN model is plotted alongside another neural network model (Joge et al., 2025) and four ESM ensembles (CNRM-ESM2-1, MIROC-ES2L, NorESM2-LM and UKESM1-0-LL), all of which explicitly modeled DMS under historical and SSP5-8.5 scenarios, spanning from 1850 to 2100 (Fig. 2 and Tables 1 and 2). DMS concentrations and fluxes in all models show a similar flat trend with different magnitudes over the historical period. For the future scenario (SSP5-8.5), four models show a decrease trend in the global annual mean DMS concentrations in the near future from 2015 to 2050 (NorESM2-MM: $-0.69\pm0.13\%$ decade^{-1}, UKESM1-0-LL: $-1.51\pm0.08\%$ decade^{-1}, Joge2025: $-0.46\pm0.03\%$ decade^{-1}, ANN: $-0.62\pm0.03\%$ decade^{-1}), and the remain two models show an increase trend (CNRM-ESM2-1: $0.41\pm0.03\%$ decade^{-1}, MIROC-ES2L: $0.82\pm0.04\%$ decade^{-1}). Subsequently, the trends remain consistent with the first half of the 21st century, with only differences in the magnitude of changes (CNRM-ESM2-1: $1.19\pm0.04\%$ decade^{-1}, MIROC-ES2L: $0.69\pm0.02\%$ decade^{-1}, NorESM2-MM: $-1.01\pm0.09\%$ decade^{-1}, UKESM1-0-LL: $-1.26\pm0.06\%$ decade^{-1}, Joge2025: $-0.58\pm0.02\%$ decade^{-1}, ANN: $-0.53\pm0.02\%$ decade^{-1}). Correspondingly, the total annual DMS emissions fluctuate within a range of 16.0–23.0 Tg S yr^{-1} under the SSP5-8.5 scenario. However, contrary to the trends of DMS concentrations, four models show an increase trend from 2015 to 2050 (CNRM-ESM2-1: $0.71\pm0.06\%$ decade^{-1}, MIROC-ES2L: $1.35\pm0.05\%$ decade^{-1}, Joge2025: $0.16\pm0.03\%$ decade^{-1}, ANN: $0.61\pm0.06\%$ decade^{-1}), and the remain two models show a decrease trend (NorESM2-MM: $-0.38\pm0.10\%$ decade^{-1}, UKESM1-0-LL: $-0.66\pm0.10\%$ decade^{-1}). While in the year from 2050 to 2100, according to specific models, the trends of DMS emissions either be amplified (CNRM-ESM2-1: $1.84\pm0.05\%$ decade^{-1}, MIROC-ES2L: $1.59\pm0.03\%$ decade^{-1}, NorESM2-MM: $-0.47\pm0.08\%$ decade^{-1}, Joge2025: $0.37\pm0.03\%$ decade^{-1},

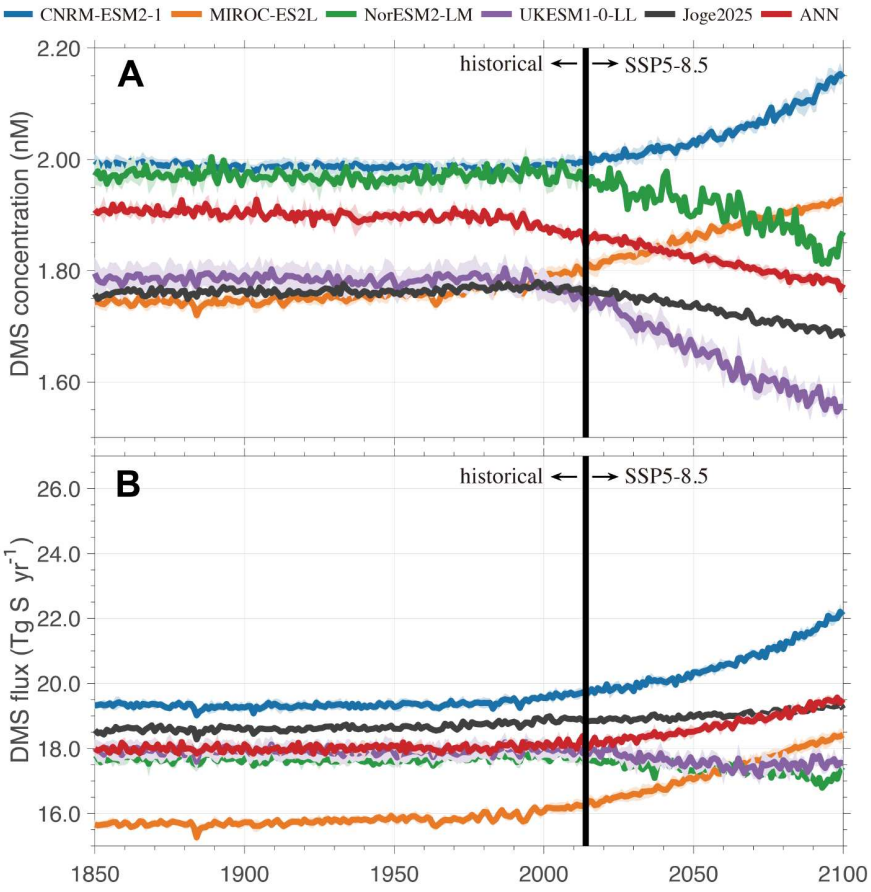

Fig. 2 Time series of global mean annual area-weighted surface ocean DMS concentration and DMS flux over 1850–2100 (CMIP6 historical and SSP5-8.5 simulations) adapted from Bock et al. (2021). (A) DMS concentration (nmol/L); (B) DMS flux (Tg S yr^{-1}), calculated using the same sea-to-air DMS flux method referenced in Joge et al. (2025). The shaded areas represent±standard deviations.

Table 1 Summary of DMS trends for historical and SSP5-8.5 scenarios over different time spans from 1850 to 2100[a)]

Model	Trend±SD % decade^{-1}				
	1850–1900	1900–1950	1950–2014	2015–2050	2050–2100
CNRM-ESM2-1	−0.06±0.01	0.02±0.01	0.06±0.01	0.41±0.03	1.19±0.04
MIROC-ES2L	−0.01±0.02	0.15±0.02	0.43±0.02	0.82±0.04	0.69±0.02
NorESM2-MM	0.02±0.04	−0.09±0.03	0.06±0.03	−0.69±0.13	−1.01±0.09
UKESM1-0-LL	0.04±0.03	−0.09±0.03	−0.18±0.03	−1.51±0.08	−1.26±0.06
Joge2025	0.07±0.02	0.01±0.02	0.06±0.02	−0.46±0.03	−0.58±0.02
this study	−0.07±0.03	−0.11±0.04	−0.31±0.03	−0.62±0.03	−0.53±0.02

a) The trends are calculated using a bootstrap method according to the method described by Joge et al. (2025). The unit is % per decade, which indicates the relative changes in DMS concentration compared to the initial year of each period.

Table 2 Summary of DMS flux trends for historical and SSP5-8.5 scenarios over different time spans from 1850 to 2100[a)]

Model	Trend±SD % decade^{-1}				
	1850–1900	1900–1950	1950–2014	2015–2050	2050–2100
CNRM-ESM2-1	−0.12±0.03	0.07±0.03	0.31±0.03	0.71±0.06	1.84±0.05
MIROC-ES2L	−0.02±0.05	0.23±0.03	0.46±0.04	1.35±0.05	1.59±0.03
NorESM2-MM	0.01±0.04	−0.05±0.04	0.11±0.03	−0.38±0.10	−0.47±0.08
UKESM1-0-LL	0.02±0.04	−0.05±0.04	0.10±0.03	−0.66±0.10	0.09±0.08
Joge2025	0.04±0.03	0.08±0.02	0.26±0.02	0.16±0.03	0.37±0.03
this study	0.02±0.05	0.10±0.04	0.14±0.03	0.61±0.06	1.06±0.04

a) The trends are calculated using a bootstrap method according to the method described by Joge et al. (2025). The unit is % per decade, which indicates the relative changes in DMS flux compared to the initial year of each period.

ANN: 1.06±0.04% decade^{-1}) or minor changes (UKESM1-0-LL: 0.09±0.08% decade^{-1}).

For future projections, our global mean concentration of surface DMS shows a decreasing trend, and the global mean sea-to-air flux of DMS exhibits an increasing trend. Both trends are consistent with those reported by Joge et al. (2025), but with a higher increasing rate for sea-to-air flux (Table 2). This increasing trend is likely due to the combined effects of decreasing ice coverage, increasing wind speed, and increasing SST, which compensate for the decreasing DMS concentration (Fig. 1). The increased wind speed in key regions such as the Arctic Ocean, Southern Ocean, and equatorial Pacific significantly elevate the gas transfer velocity (K), thereby promoting the diffusion of DMS from the ocean into the atmosphere. The decline in sea ice coverage at high latitudes not only expands the open-water area but also reduces the physical barrier to air-sea gas exchange, which further amplifies DMS release in polar regions. In addition, rising SST accelerates the volatilization of DMS. Collectively, these factors drive a substantial increase in the global mean DMS flux.

While our ANN simulations reproduce the broad global trends as those by Joge et al. (2025), spatial patterns and magnitudes diverge in several key regions. In high latitude polar regions, particularly in the Southern Ocean and the Arctic Ocean, our ANN model projects stronger DMS flux increases than those reported by Joge et al. (2025) (Fig. 1B). Conversely, in the Southern Ocean marginal seas, the combination of retreating sea ice and elevated wind speeds results in higher fluxes despite similar DMS concentrations, highlighting the dominant role of physical drivers in modulating polar DMS emissions.

3.2 Attribution of DMS changes under global warming scenario

For the eight parameters, PAR and SST exhibit an increase trend, and the other six parameters show a decrease trend under the SSP5-8.5 scenario (Fig. 3A). Globally integrated, DMS concentration decreases in the VSST test (Fig. 3B). Although elevated SST stimulates phytoplankton production especially in middle to high latitude oceans, which is the primary producer of DMS (del Valle et al., 2007; Watanabe et al., 2007; Derevianko et al., 2009; Galí et al., 2013), DMS consumption or changes in community composition appear to offset the potential increase in DMS synthesis. Distinct latitudinal disparities emerge in the trends of SST and DMS concentration. In high latitude regions such as the Southern Ocean and the Arctic Ocean, warming-induced stratification inhibits vertical nutrient supply, leading to reduced phytoplankton productivity, thereby suppressing the synthesis of DMSP (Hutchins and Tagliabue, 2024). By contrast, in low latitude regions, including the western tropical Pacific, western Indian Ocean, and West African Coast, demonstrate increased DMS concentration, this increase correlates with the proliferation of thermophilic phytoplankton (e.g., dinoflagellates), supported in some areas by localized nutrient upwelling (Lana et al., 2011).

While in the VSSS test, SSS exhibits a decreasing trend, concurrent with a declining trend of DMS concentration. Spatially, significant DMS concentration reductions are observed in the Southern Ocean and the subpolar North Atlantic, which align well with SSS trends in these regions. Whereas DMS concentration in the Arctic Ocean exhibits a slight increasing trend (Fig. 4G and Fig. S6). This is probably due to that the reduced SSS promotes stronger stratification, which limits the upwelling of nutrient-rich deep waters, thereby suppressing diatom growth (Ardyna and Arrigo, 2020). Meanwhile, DMS-productive phytoplankton (e.g., coccolithophores) that are adapted to lower SSS, enhance DMSP production and ultimately increase DMS concentration in the Arctic Ocean (Neukermans et al., 2018).

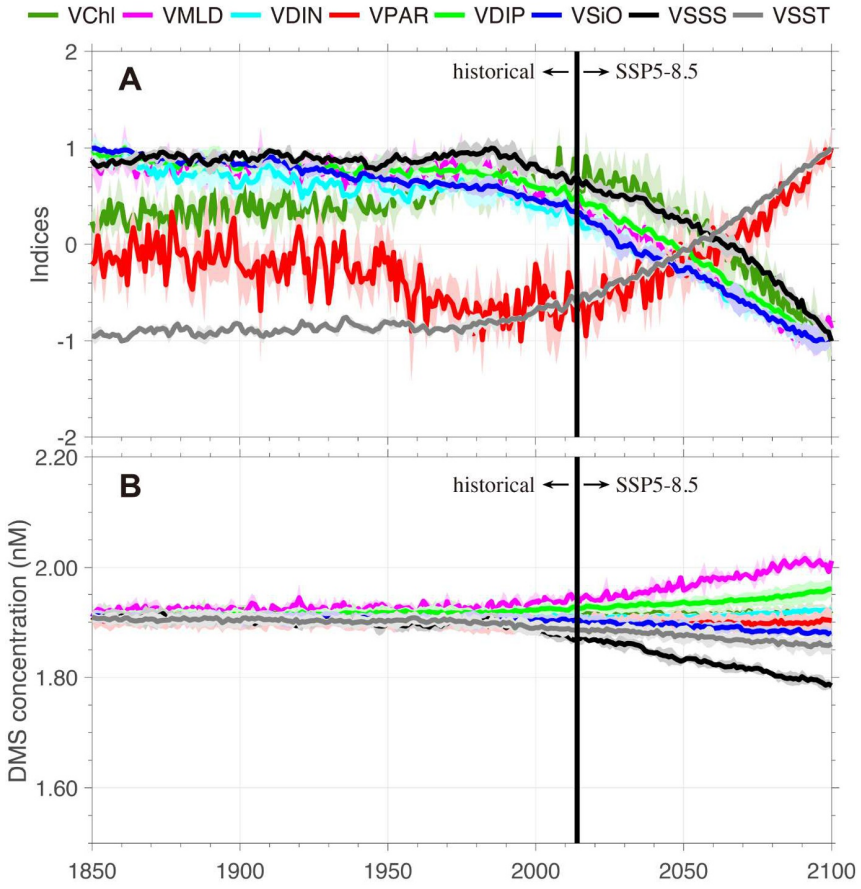

Fig. 3 Time series of input variables and DMS concentration of sensitivity tests over 1850–2100. (A) Time series of eight normalized input environmental variables scaled within the range [–1,1]; (B) Time series of global mean annual area-weighted DMS concentration of eight sensitivity tests. The shaded areas represent±standard deviations.

In the VPAR test, DMS concentration remains relatively stable, differing from the distinct decreasing trend of PAR (Fig. 3A and 3B). Low irradiance enhances bacterial consumption of DMS, at the same time reducing the proportion of high DMSP producers within assemblages (Galí et al., 2011; Vance et al., 2013; McNabb and Tortell, 2022). The two processes may offset each other, balancing the production and consumption of DMS, leading to a constant trend of DMS concentration in the VPAR test. Additionally, several regional characteristics emerge, in the high-latitude of the Southern Ocean, the increased PAR correlated with decreased DMS concentration. This is probably because the enhanced light accelerates the decomposition rate of DMS (Lim et al., 2019), and meanwhile DMS production efficiency is reduced. Conversely, minimal DMS concentration changes were observed in the North Pacific and North Indian Ocean (Fig. 4D and Fig. S6). These findings suggest that light-induced oxidative stress and inhibited microbial DMS consumption may influence regional DMS distributions. The relative contributions of biotic and abiotic processes require further *in situ* validation.

In the VMLD test, DMS concentration demonstrates a significant increasing trend globally. This observation contrasts with conventional understanding that shoaling MLD due to global warming will inhibit the upwelling of bottom nutrients (Fig. 3A), hinder the vertical mixing of higher nutrients from deeper layers and oxygen-rich waters in the upper ocean, suppressing phytoplankton primary production in low-to-middle latitude oceans and ultimately resulting in a decline of DMS concentration in the surface ocean (Sigman and Hain, 2012). Shoaling of the MLD alters light conditions in the upper ocean, confines phytoplankton to a narrower surface layer, and prolongs the residence time near the light saturation threshold (Behrenfeld and Boss, 2014; Diaz et al., 2023). The prolific DMSP producer and high light adapted taxa, such as *Synechococcus* and *Emiliania huxleyi* may become dominant. These photoacclimation processes may enhance the production of DMS (Sunda et al., 2002; Graff and Behrenfeld, 2018; Strom et al., 2020). Simultaneously, enhanced UV-B penetration in shallow MLD reduces bacterial viability, selectively inhibiting taxa that consume DMS (Wang et al., 2022). Together, the elevated DMSP synthesis coupled with suppressed microbial demethylation accounts for the observed increase in DMS concentrations. On regional scales, stabilization or localized deepening of MLD near the Antarctic continent, coupled with upwelling-induced nutrient supply, stimulates phytoplankton blooms, which subsequently drive DMS accumulation and contribute to global enhancements in DMS. In the tropical Pacific, the decline of DMS coincides with the shoaling of MLD, which aligns with former understanding. By contrast, the subtropical gyres are characterized by strong thermoclines, DMS concentration showed limited responsiveness to stratification constraints associated with the shoaling of MLD.

In the VChl test, DMS concentration remains nearly unchanged, which differs from the decreasing trend of global mean

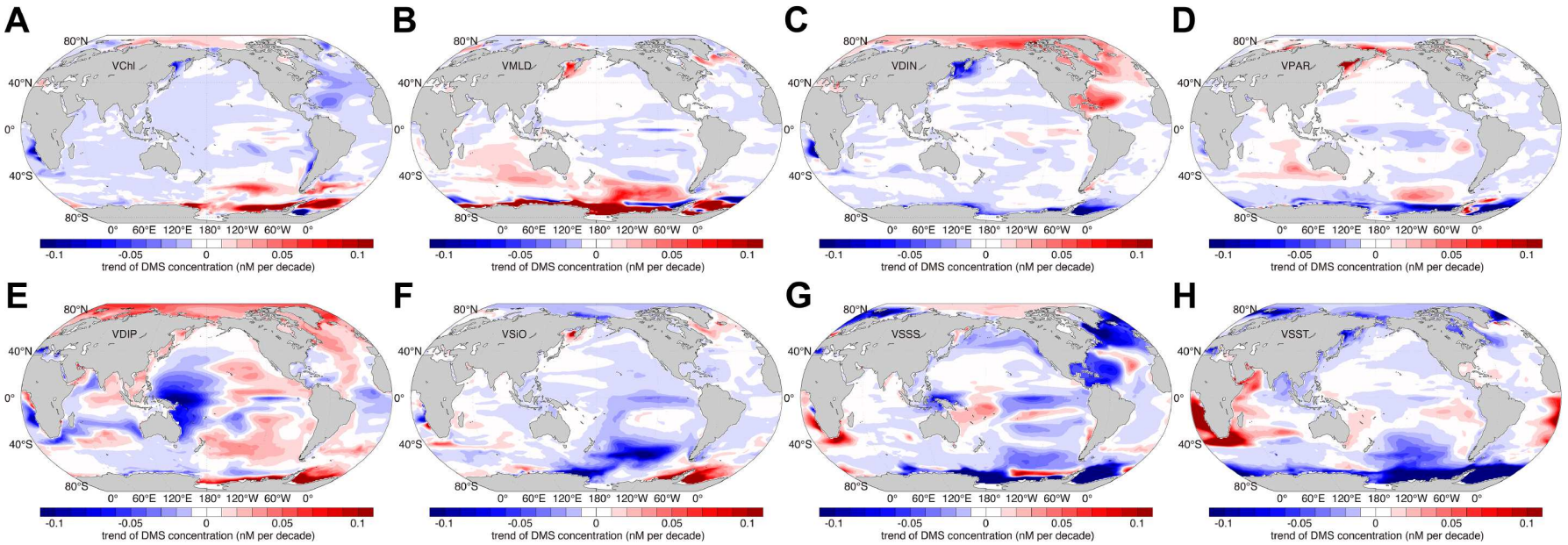

Fig. 4 Trends in DMS concentration of eight sensitivity tests under SSP5-8.5 simulations. (A) VChl; (B) VMLD; (C) VDIN; (D) VPAR; (E) VDIP; (F) VSiO; (G) VSSS; (H) VSST.

Chl a concentration. This is in contrast to previous studies that extensively link DMS to Chl a, and indicates that the biogeochemical cycle of DMS is far more complex than Chl a can represent (Simó and Dachs, 2002; Nemcek et al., 2008; Galí and Simó, 2015). Indeed, applying an algorithm based on Chl a yielded little insight into DMS dynamics (Hirata et al., 2011). One likely explanation for this decoupling is the substantial variation in DMSP production among phytoplankton taxa. High DMSP producers such as coccolithophore constitutes high intracellular DMSP concentrations, whereas low producers, including most diatoms, contribute less despite comparable biomass levels (Sunda et al., 2007; McParland and Levine, 2019). In addition, the fact that Chl a represents a composite signal from all phytoplankton taxa, may have limited utility in predicting the spatial patterns of DMS on a global scale, but may be useful regionally.

For nutrient tests, DMS concentrations exhibit increasing trends in VDIN and VDIP tests, despite both surface DIN and DIP concentrations decreasing under the SSP5-8.5 scenario. Overall, the DMS–nutrients relationship can be partially attributed to the sulfur overflow hypothesis (Stefels, 2000), which suggests that nutrient-limited phytoplankton increase DMSP production, and its subsequent cleavage to DMS, which serves as a mechanism to regulate intracellular sulfur quotas when protein synthesis is limited (Stefels, 2000; Simó and Vila-Costa, 2006; Hatton and Wilson, 2007; Spiese and Tatarkov, 2014; Kinsey et al., 2016). This hypothesis can also explain the elevated DMS concentrations in the Southern Ocean, the subpolar North Atlantic, and the Bering Sea, where nutrients show decreasing trends (Fig. S6). Moreover, nutrient-dependent effects explain seasonal variability, particularly as phytoplankton growth becomes nutrient-limited during summer time (Behrenfeld and Boss, 2014; Browning and Moore, 2023). Beyond this cellular physiological response, nutrient limitation may also change the phytoplankton community toward taxa that are inherently high DMSP producers, thereby amplifying DMS release at the community level (Stefels et al., 2007; Archer et al., 2009; McParland and Levine, 2019). Moreover, the contribution of marine bacteria to DMSP/DMS production and consumption cannot be disregarded, as their metabolic pathways are similarly sensitive to changes in nutrients (Reisch et al., 2011). For instance, nitrogen limitation can enhance the activity of bacterial DMSP lyase enzymes, thereby increasing DMS production (Sunda et al., 2007; Zindler et al., 2012). Certain phytoplankton (e.g., dinoflagellates) may similarly increase the production of DMSP under phosphorus limitation, further promoting DMS production (Keller and Korjeff-Bellows, 1996). These interacting mechanisms explain why DMS concentrations increase when DIN and DIP decrease, highlighting the importance of integrating physiological and ecological drivers in biogeochemical assessments.

The ocean represents an intricate system where environmental changes directly modulate DMS concentrations. The elevated SST and PAR will strengthen ocean stratification under the global warming scenario (SSP5-8.5), then shoaling the MLD and reducing nutrient supplies from the deep ocean. Our findings suggest that these effects jointly determine the temporal variation of DMS concentrations.

3.3 Key factors regulating DMS variation in typical regions

To further investigate the drivers of regional DMS variabilities, we divide the ocean into six regions according to Longhurst (1998): Polar North, polar South, westerlies North, westerlies South, trades, and coastal (see Fig. S1). We then examined the key factors influencing DMS concentrations across these regions for both historical and SSP5-8.5 periods (Fig. 5). For each of the six typical regions, corresponding gridded datasets of environmental variables and DMS concentrations were systematically extracted, and then we calculated the correlation coefficients for both periods, and the correlation coefficients for both the historical and future periods were statistically significant (p <0.05).

No key driving factors of DMS variation are identified in the westerlies South regions both in historical and SSP5-8.5 periods (all the correlation coefficients with environmental parameters are lower than 0.3), this likely reflects that these areas encompass diverse biomes with site-specific drivers. When analyzed as a whole, no single dominant factor was identified. In contrast, DMS concentrations in the westerlies North region show negative correlations with DIP in the historical (r=−0.66) and SSP5-8.5 period (r=−0.57), and positive correlations with SSS (r=0.68 and r=0.65) in the two periods. These results suggest that low nutrient levels may favor small phytoplankton or *Phaeocystis*, which are more prolific DMS producers compared to diatoms (Wang et al., 2018).

In the polar South, a strong negative correlation is observed between PAR and predicted DMS concentrations (r=–0.69 and r=−0.71, respectively), and a slightly negative correlation with SST (r=−0.55 and r=−0.61, respectively). The polar South region is characterized by high background nutrient concentrations and deep mixed layers (Browning and Moore, 2023; Treguier et al., 2025). Under the future scenario (SSP5-8.5), the rising SST shoals the MLD, leading to a gradual depletion of surface nutrients and consequently limiting phytoplankton growth (Fig. S6), which ultimately diminishes the production efficiency of DMS (Simó and Pedrós-Alió, 1999; Bopp et al., 2005; Doney, 2006).

In the polar North region, DMS shows the strongest negative correlation with DIP (r=−0.32) in the historical period, whereas the strongest positive correlation is with SiO (r=0.39) in the high-emission scenario among all environmental variables. These observed patterns likely reflect the changes in the Arctic biome driven by climate change (warming). Additional evidence emerges from changing relationships between Chl a and DMS concentration, transitioning from a weakly positive correlation (r=0.17) in the historical scenario to a slightly negative correlation (r=−0.07) in the projected future scenario. Regarding the physical environmental parameters, both SST and PAR consistently exhibit positive correlations with simulated DMS concentrations in the two scenarios. This suggests that the elevated SST and PAR in the Arctic Ocean may enhance biological productivity, thereby promoting DMS production (Vallina and Simó, 2007; Galí et al., 2015; Galí and Simó, 2015).

Although polar ecosystems exhibit evolutionarily conserved DMSP metabolic pathways and analogous physiological functions, these sulfur metabolism systems neither demonstrate convergent DMS emission profiles nor uniform environmental response mechanisms. In the polar North, DMS are primarily regulated by freshwater inputs, nutrient stoichiometry and light conditions, which collectively modulate phytoplankton community structure and DMSP lyase activity (Levasseur, 2013; Hayashida et al., 2020). In contrast, the Southern Ocean is

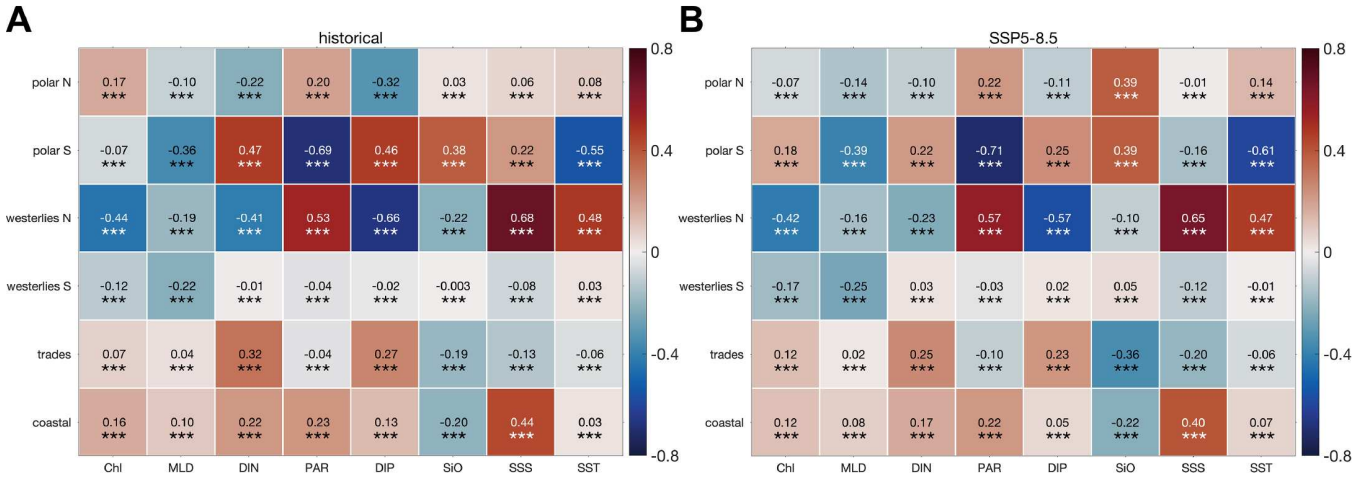

Fig. 5 Regional correlations of DMS concentration with eight environmental variables in six main regions. (A) Correlations of DMS concentration with eight input environmental variables under historical scenario; (B) Correlations of DMS concentration with eight input environmental variables under SSP5-8.5 scenario. *** represents a *p*-value lower 0.05 ($p<0.05$).

influenced by iron limitation, circumpolar circulation and seasonal sea-ice cycles, driving phytoplankton succession between *Phaeocystis*-dominated blooms (high DMSP producers) and diatom-dominated processes (Nissen and Vogt, 2021; Zhang et al., 2023). These distinct regulatory mechanisms indicate a fundamental functional asymmetry between the polar North and the polar South.

In coastal regions, SSS stands out as a prominent influencing factor among all eight environmental variables, showing a positive correlation with DMS both in the historical (r=0.44) and SSP5-8.5 (r=0.40) periods. The elevated SSS in coastal regions often indicates reduced freshwater input, which also limits the supply of nutrients essential for diatom growth (Horn et al., 2023). Concurrently, the increased stratification selectively promotes the growth of algae (e.g., dinoflagellates), leading to changes in phytoplankton community structure from low-DMSP-yielding diatoms to high-DMSP-producing dinoflagellates (Hatton et al., 2012; Wells et al., 2020; Galí et al., 2021; Zhang et al., 2024). Therefore, the prolific DMSP producers boost the total DMSP inventory, consequently enhancing the DMS production (Simó, 2001; Stefels et al., 2007). In contrast, within the trades region (open ocean), where nutrient levels are generally low and small phytoplankton dominate, DMS concentrations are positively correlated with DIN, DIP, and Chl a (Wang et al., 2020; Zhang et al., 2024). This suggests that in the trades, nutrient-driven higher primary production leads to higher DMS production (Dani and Loreto, 2017).

Observational and modeling studies have extensively documented the distribution of DMS concentrations and sea-to-air fluxes across the global ocean (Simó et al., 2002; Lana et al., 2012; Galí et al., 2015; Séférian et al., 2020; Joge et al., 2025). These studies indicate that sea-to-air DMS flux is not solely governed by global biogeochemical cycles but also influenced by complex ecological interactions, planktonic food-web dynamics, cellular physiological processes, and marine chemical transformations (Simó et al., 2002). Notably, the elevated sea-to-air DMS fluxes are predominantly observed in upwelling zones, particularly in the tropical and equatorial Pacific Ocean, and DMS flux peaks in the trades region (>10 Tg S yr^{-1}). While the polar and coastal areas are also notable emission hotspots, with their emissions projected to increase most significantly in the future scenario (25.13% in Polar North, 13.89% in Polar South and 18.32% in coastal), and the growth rate is significantly higher than that in the other three regions (1.27% in westerlies North, 4.28% in westerlies South and 7.70% in trades) (Fig. 6).

Furthermore, recent research highlights the influence of SST, deep-water formation, biological productivity, and thermohaline circulation on the variability of DMS flux (Séférian et al., 2020). Our results demonstrate that DMS concentrations exhibit regional-scale dependence on multiple environmental drivers (Fig. 7). In the DMS production pathway, phytoplankton-derived dissolved DMS is subject to negative regulation by nutrient availability (DIN, DIP, SiO) and MLD. The subsequent conversion of dissolved DMS to its gaseous form and its emission into the atmosphere are modulated by SST and SSW (positive correlation) with sea ice coverage (negative correlation). Moreover, within the climate feedback loop, atmospheric DMS undergoes oxidation to form non-sea-salt sulfates ($NSS\text{-}SO_4^{2-}$), which serve as CCN. This process enhances cloud albedo, reduces incoming solar radiation (positive forcing), and ultimately lowers SST (negative forcing), thereby establishing a negative climate feedback mechanism.

Moving forward, the incorporation of regionally resolved biogeochemical mechanisms, coupled with an improved representation of DMS production and consumption processes within machine learning frameworks, may be achieved through the independent training of models for discrete biogeographical provinces. Such an approach holds the potential to more accurately resolve the intrinsic nonlinear dynamics governing DMS variability. In addition, attaining a more accurate characterization of regional patterns will be essential for constraining uncertainties in projected oceanic sulfur fluxes under climate change scenarios.

4. Conclusions

The comparison of DMS concentrations and flux variations over the simulation periods from 1850 to 2100 (historical and SSP5-8.5 for CMIP6 ESMs) yields two key insights. Firstly, all models

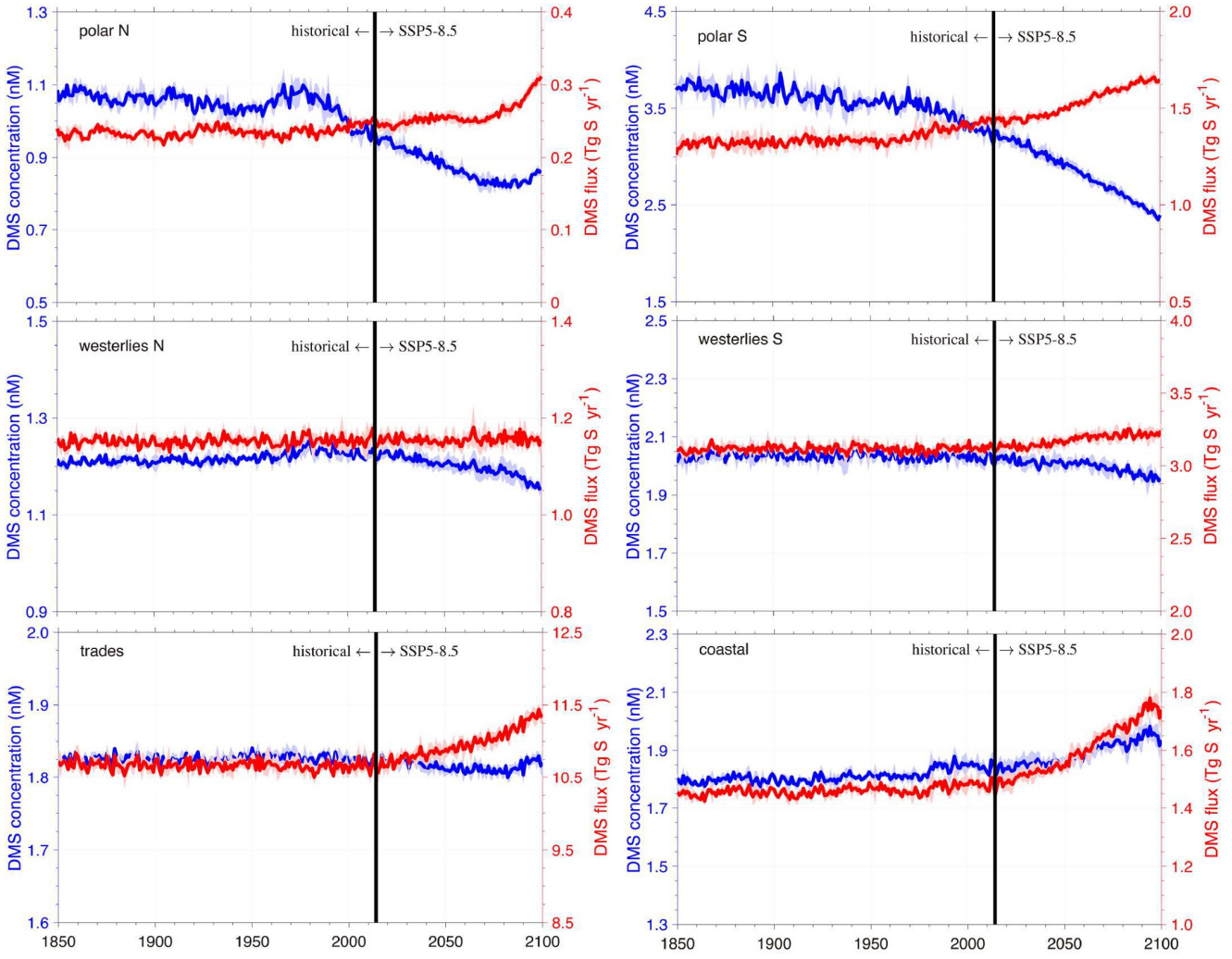

Fig. 6 Time series of regional mean annual area-weighted DMS concentration and DMS flux in six main regions spanning 1850–2100 (historical and SSP5-8.5 simulations). The shaded areas represent±standard deviations.

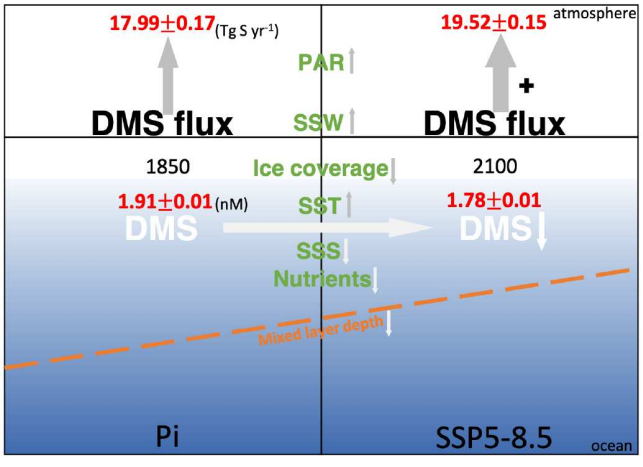

Fig. 7 A schematic diagram illustrates the interactions between DMS and environmental parameters. Under SSP5-8.5 scenario, the elevated SST enhances ocean stratification, resulting in a shallower MLD and thereby limiting nutrients supply. Concurrently, the increased PAR intensifies the photochemical degradation of DMS, further suppressing surface DMS concentrations. Moreover, higher SST and SSW, along with the declining sea ice coverage in high-latitude regions promote the sea-to-air emission of DMS, leading to an increased DMS flux into the atmosphere.

demonstrate relative stability during the historical period. In contrast, in future simulations, two ESMs (CNRM-ESM2-1 and MIROC-ES2L) exhibit concurrent increases in surface ocean DMS concentrations and flux. The remaining four models show divergent trends, NorESM2-LM and UKESM1-0-LL project decreases in both DMS concentrations and flux, whereas ANN and Joge2025 simulate decreasing DMS concentrations accompanied by increasing flux, indicating a partial decoupling between DMS concentrations and emissions. Although ESMs or non-linear equations may not fully elucidate the relationship between DMS and marine phytoplankton, clarifying its response to climate change is crucial.

Secondly, our findings suggest that DMS concentrations exhibit regional-scale dependence on multiple environmental drivers. In the trades region (open ocean), higher DMS production is primarily driven by nutrient-mediated increases in primary productivity. Conversely, in the westerlies North region, DMS concentrations display negative correlations with Chl a, DIN, DIP, and SiO, while showing strong positive correlations with PAR, SSS, and SST. A strong negative correlation is observed between PAR/SST and DMS in the polar South during both historical and future periods, while slightly

positive correlations with DIN, DIP, and SiO. Moreover, in the coastal regions, SSS is identified as a key positive predictor of DMS concentrations than other parameters. In contrast, no strong correlations with DMS are observed for any factors in the westerly South.

Our results demonstrate that variations in DMS concentration are rarely unidirectional in response to isolated changes in a single environmental parameter (Fig. 7). This highlights the complex interactions among these environmental factors, which cannot be adequately captured by a linear regression model. Future work should focus on the combined effects, using observational data to constrain models, and integrating these with ESMs to more accurately simulate DMS concentrations under different scenarios. It is also crucial to consider the potential climatic implications of changes in DMS production driven by biogeochemical factors when projecting future climate change.

Acknowledgement

We thank the observational DMS community for making their measurements publicly available. We also thank the authors and agencies for providing the ancillary data used in this study. This work was supported by the National Key Research and Development Program of China (Grant No. 2025YFF0517304) and the Natural Science Foundation of Fujian Province of China (Grant No. 2023J02001).

Supporting information

The supporting information is available online at http://earth.scichina.com and http://link.springer.com. The supporting materials are published as submitted, without typesetting or editing. The responsibility for scientific accuracy and content remains entirely with the authors.

Compliance and ethics

The authors declare no conflict of interest.

References

Archer S D, Cummings D G, Llewellyn C A, et al. 2009. Phytoplankton taxa, irradiance and nutrient availability determine the seasonal cycle of DMSP in temperate shelf seas. Mar Ecol Prog Ser, 394: 111–124

Ardyna M, Arrigo K R. 2020. Phytoplankton dynamics in a changing Arctic Ocean. Nat Clim Chang, 10: 892–903

Behrenfeld M J, Boss E S. 2014. Resurrecting the ecological underpinnings of ocean plankton blooms. Annu Rev Mar Sci, 6: 167

Bock J, Michou M, Nabat P, et al. 2021. Evaluation of ocean dimethylsulfide concentration and emission in CMIP6 models. Biogeosciences, 18: 3823–3860

Bopp L, Aumont O, Belviso S, et al. 2003. Potential impact of climate change on marine dimethyl sulfide emissions. Tellus B-Chem Phys Meteorol, 55: 11–22

Bopp L, Aumont O, Cadule P, et al. 2005. Response of diatoms distribution to global warming and potential implications: A global model study. Geophys Res Lett, 32: 2005GL023653

Breiman L. 2001. Random Forests. Mach Learn, 45: 5–32

Browning T J, Moore C M. 2023. Global analysis of ocean phytoplankton nutrient limitation reveals high prevalence of co-limitation. Nat Commun, 14: 5014

Charlson R J, Lovelock J E, Andreae M O, et al. 1987. Oceanic phytoplankton, atmospheric sulphur, cloud albedo and climate. Nature, 326: 655–661

Danabasoglu G, Lamarque J-F, Bacmeister J, et al. 2020. The Community Earth System Model version 2 (CESM2). J Adv Model Earth Syst, 12: e2019MS001916

Dani K G S, Loreto F. 2017. Trade-Off between dimethyl sulfide and isoprene emissions from marine phytoplankton. Trends Plant Sci, 22: 361–372

del Valle D A, Kieber D J, John B, et al. 2007. Light-Stimulated production of dissolved DMSO by a particle-associated process in the Ross Sea, Antarctica. Limnol Oceanogr, 52: 2456–2466

Derevianko G J, Deutsch C, Hall A. 2009. On the relationship between ocean DMS and solar radiation. Geophys Res Lett, 36: 2009GL039412

Diaz B P, Zelzion E, Halsey K, et al. 2023. Marine phytoplankton downregulate core photosynthesis and carbon storage genes upon rapid mixed layer shallowing. ISME J, 17: 1074–1088

Doney S C. 2006. Plankton in a warmer world. Nature, 444: 695–696

Gabric A, Qu B, Rotstayn L, et al. 2013. Global simulations of the impact on contemporary climate of a perturbation to the sea-to-air flux of dimethylsulfide. AMOJ, 63: 365–376

Galí M, Saló V, Almeda R, et al. 2011. Stimulation of gross dimethylsulfide (DMS) production by solar radiation. Geophys Res Lett, 38: 2011GL048051

Galí M, Simó R, Vila-Costa M, et al. 2013. Diel patterns of oceanic dimethylsulfide (DMS) cycling: Microbial and physical drivers. Glob Biogeochem Cycle, 27: 620–636

Galí M, Simó R. 2015. A meta-analysis of oceanic DMS and DMSP cycling processes: Disentangling the summer paradox. Glob Biogeochem Cycle, 29: 496–515

Galí M, Devred E, Levasseur M, et al. 2015. A remote sensing algorithm for planktonic dimethylsulfoniopropionate (DMSP) and an analysis of global patterns. Remote Sens Environ, 171: 171–184

Galí M, Lizotte M, Kieber D J, et al. 2021. DMS emissions from the Arctic marginal ice zone. Elementa-Sci Anthropocene, 9: 00113

Gardner M W, Dorling S R. 1998. Artificial neural networks (the multilayer perceptron)—A review of applications in the atmospheric sciences. Atmos Environ, 32: 2627–2636

Graff J R, Behrenfeld M J. 2018. Photoacclimation responses in subarctic atlantic phytoplankton following a natural mixing-restratification event. Front Mar Sci, 5: 209

Hamilton D S, Lee L A, Pringle K J, et al. 2014. Occurrence of pristine aerosol environments on a polluted planet. Proc Natl Acad Sci USA, 111: 18466–18471

Hatton A D, Wilson S T. 2007. Particulate dimethylsulphoxide and dimethylsulphoniopropionate in phytoplankton cultures and Scottish coastal waters. Aquat Sci, 69: 330–340

Hatton A D, Shenoy D M, Hart M C, et al. 2012. Metabolism of DMSP, DMS and DMSO by the cultivable bacterial community associated with the DMSP-producing dinoflagellate *Scrippsiella trochoidea*. Biogeochemistry, 110: 131–146

Hayashida H, Carnat G, Galí M, et al. 2020. Spatiotemporal variability in modeled bottom ice and sea surface dimethylsulfide concentrations and fluxes in the Arctic during 1979–2015. Glob Biogeochem Cycle, 34: e2019GB006456

Hirata T, Hardman-Mountford N J, Brewin R J W, et al. 2011. Synoptic relationships between surface chlorophyll-a and diagnostic pigments specific to phytoplankton functional types. Biogeosciences, 8: 311–327

Horn H G, van Rijswijk P, Soetaert K, et al. 2023. Drivers of spatial and temporal micro- and mesozooplankton dynamics in an estuary under strong anthropogenic influences (the Eastern Scheldt, Netherlands). J Sea Res, 192: 102357

Hulswar S, Simó R, Galí M, et al. 2022. Third revision of the global surface seawater dimethyl sulfide climatology (DMS-Rev3). Earth Syst Sci Data, 14: 2963–2987

Hutchins D A, Tagliabue A. 2024. Feedbacks between phytoplankton and nutrient cycles in a warming ocean. Nat Geosci, 17: 495–502

Joge S D, Mansour K, Simó R, et al. 2025. Climate warming increases global oceanic dimethyl sulfide emissions. Proc Natl Acad Sci USA, 122: e2502077122

Keller M D, Korjeff-Bellows W. 1996. Physiological aspects of the production of dimeyhtlsulfoniopropionate (DMSP) by marine phytoplankton. In: Kiene R P, Visscher P T, Keller M D, et al., eds. Biological and Environmental Chemistry of DMSP and Related Sulfonium Compounds. New York: Plenum Press. 131–142

Kinsey J D, Kieber D J, Neale P J. 2016. Effects of iron limitation and UV radiation on *Phaeocystis antarctica* growth and dimethylsulfoniopropionate, dimethylsulfoxide and acrylate concentrations. Environ Chem, 13: 195–211

Lana A, Bell T G, Simó R, et al. 2011. An updated climatology of surface dimethlysulfide concentrations and emission fluxes in the global ocean. Glob Biogeochem Cycle, 25: 1

Lana A, Simó R, Vallina S M, et al. 2012. Re-Examination of global emerging patterns of ocean DMS concentration. Biogeochemistry, 110: 173–182

Levasseur M. 2013. Impact of Arctic meltdown on the microbial cycling of sulphur. Nat Geosci, 6: 691–700

Lim A S, Jeong H J, Ok J H, et al. 2019. Effects of light intensity and temperature on growth and ingestion rates of the mixotrophic dinoflagellate *Alexandrium pohangense*. Mar Biol, 166: 98

Liss P S, Slater P G. 1974. Flux of gases across the air-sea interface. Nature, 247: 181–184

Longhurst A R. 1998. Ecological Geography of the Sea. San Diego: Academic Press

McNabb B J, Tortell P D. 2022. Improved prediction of dimethyl sulfide (DMS) distributions in the northeast subarctic Pacific using machine-learning algorithms. Biogeosciences, 19: 1705–1721

McParland E L, Levine N M. 2019. The role of differential DMSP production and community composition in predicting variability of global surface DMSP concentrations. Limnol Oceanogr, 64: 757–773
Nemcek N, Ianson D, Tortell P D. 2008. A high-resolution survey of DMS, CO_2, and O_2/Ar distributions in productive coastal waters. Glob Biogeochem Cycle, 22: 2006GB002879
Neukermans G, Oziel L, Babin M. 2018. Increased intrusion of warming Atlantic water leads to rapid expansion of temperate phytoplankton in the Arctic. Glob Change Biol, 24: 2545–2553
Nissen C, Vogt M. 2021. Factors controlling the competition between *Phaeocystis* and diatoms in the Southern Ocean and implications for carbon export fluxes. Biogeosciences, 18: 251–283
O'Neill B C, Tebaldi C, van Vuuren D P, et al. 2016. The Scenario Model Intercomparison Project (ScenarioMIP) for CMIP6. Geosci Model Dev, 9: 3461–3482
Quinn P K, Bates T S. 2011. The case against climate regulation via oceanic phytoplankton sulphur emissions. Nature, 480: 51–56
Reisch C R, Moran M A, Whitman W B. 2011. Bacterial catabolism of dimethylsulfoniopropionate (DMSP). Front Microbio, 2: 1
Schmidtko S, Johnson G C, Lyman J M. 2013. MIMOC: A global monthly isopycnal upper-ocean climatology with mixed layers. J Geophys Res-Oceans, 118: 1658–1672
Séférian R, Berthet S, Yool A, et al. 2020. Tracking improvement in simulated marine biogeochemistry between CMIP5 and CMIP6. Curr Clim Change Rep, 6: 95–119
Sigman D M, Hain M P. 2012. The biological productivity of the ocean. Nat Educ Knowl, 3: 1–16
Simó R, Pedrós-Alió C. 1999. Short-Term variability in the open ocean cycle of dimethylsulfide. Glob Biogeochem Cycle, 13: 1173–1181
Simó R. 2001. Production of atmospheric sulfur by oceanic plankton: Biogeochemical, ecological and evolutionary links. Trends Ecol Evol, 16: 287–294
Simó R, Dachs J. 2002. Global ocean emission of dimethylsulfide predicted from biogeophysical data. Glob Biogeochem Cycle, 16, doi: 10.1029/2001gb001829
Simó R, Archer S D, Pedrós-Alió C, et al. 2002. Coupled dynamics of dimethylsulfoniopropionate and dimethylsulfide cycling and the microbial food web in surface waters of the North Atlantic. Limnol Oceanogr, 47: 53–61
Simó R, Vila-Costa M. 2006. Ubiquity of algal dimethylsulfoxide in the surface ocean: Geographic and temporal distribution patterns. Mar Chem, 100: 136–146
Six K D, Kloster S, Ilyina T, et al. 2013. Global warming amplified by reduced sulphur fluxes as a result of ocean acidification. Nat Clim Change, 3: 975–978
Spiese C E, Tatarkov E A. 2014. Dimethylsulfoxide reduction activity is linked to nutrient stress in *Thalassiosira pseudonana* NCMA 1335. Mar Ecol Prog Ser, 507: 31–38
Stefels J. 2000. Physiological aspects of the production and conversion of DMSP in marine algae and higher plants. J Sea Res, 43: 183–197
Stefels J, Steinke M, Turner S, et al. 2007. Environmental constraints on the production and removal of the climatically active gas dimethylsulphide (DMS) and implications for ecosystem modelling. Biogeochemistry, 83: 245–275
Strom S L, Barberi O, Mazur C, et al. 2020. High light stress reduces dinoflagellate predation on phytoplankton through both direct and indirect responses. Aquat Microb Ecol, 84: 43–57
Sunda W, Kieber D J, Kiene R P, et al. 2002. An antioxidant function for DMSP and DMS in marine algae. Nature, 418: 317–320
Sunda W G, Hardison R, Kiene R P, et al. 2007. The effect of nitrogen limitation on cellular DMSP and DMS release in marine phytoplankton: Climate feedback implications. Aquat Sci, 69: 341–351
Treguier A M, de Boyer Montégut C, Yeager S, et al. 2025. Multidecadal trends of the mixed layer depth and their relation to the wind in global ocean models forced by an atmospheric reanalysis. J Geophys Res-Oceans, 130: e2024JC022271
Vallina S M, Simó R. 2007. Strong relationship between DMS and the solar radiation dose over the global surface ocean. Science, 315: 506–508
Vance T R, Davidson A T, Thomson P G, et al. 2013. Rapid DMSP production by an Antarctic phytoplankton community exposed to natural surface irradiances in late spring. Aquat Microb Ecol, 71: 117–129
Wang S, Maltrud M E, Burrows S M, et al. 2018. Impacts of shifts in phytoplankton community on clouds and climate via the sulfur cycle. Glob Biogeochem Cycle, 32: 1005–1026
Wang T, Huang Q, Burns A S, et al. 2022. Oxidative stress regulates a pivotal metabolic switch in dimethylsulfoniopropionate degradation by the marine bacterium ruegeria pomeroyi. Microbiol Spectr, 10: e03191-22
Wang W L, Song G, Primeau F, et al. 2020. Global ocean dimethyl sulfide climatology estimated from observations and an artificial neural network. Biogeosciences, 17: 5335–5354
Watanabe Y W, Yoshinari H, Sakamoto A, et al. 2007. Reconstruction of sea surface dimethylsulfide in the North Pacific during 1970s to 2000s. Mar Chem, 103: 347–358
Webb A L, Malin G, Hopkins F E, et al. 2016. Ocean acidification has different effects on the production of dimethylsulfide and dimethylsulfoniopropionate measured in cultures of *Emiliania huxleyi* and a mesocosm study: A comparison of laboratory monocultures and community interactions. Environ Chem, 13: 314–329
Wells M L, Karlson B, Wulff A, et al. 2020. Future HAB science: Directions and challenges in a changing climate. Harmful Algae, 91: 101632
Zhang Y, Zhao W, Wei H, et al. 2023. Iron limitation and uneven grazing pressure on phytoplankton co-lead the seasonal species succession in the Ross Ice Shelf Polynya. J Geophys Res-Oceans, 128: e2022JC019026
Zhang H Q, Yu J, Lai J G, et al. 2024. Influence of the community assemblage on sulfur distributions in the South China Sea. Mar Environ Res, 197: 106481
Zhao J, Zhang Y, Bie S, et al. 2024. Changes in global DMS production driven by increased CO_2 levels and its impact on radiative forcing. NPJ Clim Atmos Sci, 7: 18
Zindler C, Peeken I, Marandino C A, et al. 2012. Environmental control on the variability of DMS and DMSP in the Mauritanian upwelling region. Biogeosciences, 9: 1041–1051

(Editorial Handling: Xiaoxue WANG)